J Ind Microbiol Biotechnol (2012) 39:927–941
DOI 10.1007/s10295-012-1090-4

SYSTEMS BIOTECHNOLOGY

Quantification of metabolism in *Saccharomyces cerevisiae* under hyperosmotic conditions using elementary mode analysis

Jignesh H. Parmar · Sharad Bhartiya · K. V. Venkatesh

Received: 19 December 2010 / Accepted: 14 January 2012 / Published online: 22 February 2012

Abstract Yeast metabolism under hyperosmotic stress conditions was quantified using elementary mode analysis to obtain insights into the metabolic status of the cell. The fluxes of elementary modes were determined as solutions to a linear program that used the stoichiometry of the elementary modes as constraints. The analysis demonstrated that distinctly different sets of elementary modes operate under normal and hyperosmotic conditions. During the adaptation phase, elementary modes that only produce glycerol are active, while elementary modes that yield biomass, ethanol, and glycerol become active after the adaptive phase. The flux distribution in the metabolic network, calculated using the fluxes in the elementary modes, was employed to obtain the flux ratio at key nodes. At the glucose 6-phosphate (G6P) node, 25% of the carbon influx was diverted towards the pentose phosphate pathway under normal growth conditions, while only 0.3% of the carbon flux was diverted towards the pentose phosphate pathway during growth at 1 M NaCl, indicating that cell growth is arrested under hyperosmotic conditions. Further, objective functions were used in the linear program to obtain optimal solution spaces corresponding to the different accumulation rates. The analysis demonstrated that while biomass formation was optimal under normal growth conditions, glycerol synthesis was closer to optimal during adaptation to osmotic shock.

Keywords Yeast · Central metabolism · Hyperosmotic stress · Elementary mode analysis · Optimal feasible space

Introduction

Studying metabolic pathways is an essential task when attempting to characterize the phenotypic behavior of living cells. Metabolic networks are typically characterized by quantifying the reaction rates that prevail in the network. However, the accurate dynamic modeling of metabolic reactions is usually not feasible due to difficulties in acquiring kinetic rate expressions. Therefore, alternative network-based approaches have been developed that have been found to be useful for establishing the fluxes through the network. In contrast to dynamic models, these descriptions only require knowledge of the network topology and stoichiometry, which are well known in several cases. One such network-based approach is elementary mode analysis (EMA), as developed by Schuster and co-workers [25, 26]. Elementary modes (EM) are minimal sets of reactions that can operate at the steady state in a metabolic network [19, 23, 25]. The term "minimal set of reactions" implies that if any enzyme belonging to a particular set is nonoperational then it would lead to the cessation of the steady-state flux through that specific elementary mode. EMA has proven to be useful for a number of biochemical applications, such as interpreting metabolic network functions [7, 9, 21], assessing the robustness and fragility of cellular functions [13, 14, 31], and improving strain performance [6, 28]. Elementary modes can also be used to determine the fluxes of the entire

Electronic supplementary material The online version of this article (doi:10.1007/s10295-012-1090-4) contains supplementary material, which is available to authorized users.

J. H. Parmar · S. Bhartiya · K. V. Venkatesh (✉)
Department of Chemical Engineering, Indian Institute of Technology, Bombay, Powai, Mumbai 400076, India
e-mail: venks@che.iitb.ac.in

S. Bhartiya
e-mail: bhartiya@che.iitb.ac.in

metabolic network using matrix algebra [8]. Recently, it has also been shown that EMA can provide the basis for describing and understanding the properties of signaling and transcriptional regulatory networks [10, 15]. Here, we report the utilization of elementary mode analysis to quantify the metabolic network of *Saccharomyces cerevisiae* under hyperosmotic shock.

The yeast *S. cerevisiae* has evolved specific mechanisms to survive under various kinds of stresses such as osmotic stress, oxidative stress, starvation, and radiation stress by changing its intracellular network status. Among these stresses, the metabolic and signaling pathways involved in the adaptation to osmotic stress have been well characterized [1–4, 12]. Upon hyperosmotic shock, the yeast cell loses water due to the osmotic imbalance across the cell membrane, resulting in cell shrinkage and thus arrested cellular activity [1]. To survive such life threatening cues, yeast cells synthesize and accumulate glycerol, a so-called compatible solute or osmolyte, which can stabilize various enzymes and restore the cell turgor pressure required for cell growth [3]. In *S. cerevisiae*, the osmotic upshift triggers a signaling pathway known as the high osmolarity glycerol (HOG) pathway [4, 11], which in turn regulates several genes in the metabolic pathway. In *S. cerevisiae*, the genetic remodeling ultimately results in the increased production and accumulation of chemically inert osmolytes, mainly glycerol [22]. Thus, the cell has to modify its metabolism to cope with such an environmental cue by synthesizing glycerol at the expense of biomass and other byproducts. It is therefore of interest to analyze the metabolic flux distribution for the growth of yeast under the conditions of osmotic shock, and to compare this distribution with that obtained under normal growth. We use the EMA approach to obtain fluxes under normal and stress conditions. Our results indicate that distinctly different sets of elementary modes are operational under normal and hyperosmotic conditions. The analysis further indicates that cell growth is optimal under normal growth conditions and suboptimal under osmotic stress.

Mathematical method

The metabolic network of *S. cerevisiae* consists of transport processes as well as the core catabolism and anabolism (including glycerol synthesis reactions), resulting in more than a thousand reactions. However, in the context of osmotic stress, only the central carbon metabolism is of primary interest. The metabolic model for the central carbon metabolism based on information provided by the literature [5, 29, 30] includes glycolytic reactions, the TCA cycle, and the pentose phosphate pathway (see Table S2 of the Electronic supplementary material, ESM). As our main focus is on the distribution of carbon into the biomass and glycerol, we do not consider the compartmentalization of the TCA cycle. The biomass is represented in terms of equivalent stoichiometric quantities of biosynthetic precursors [5]. The metabolism incorporates the uptakes of glucose and oxygen as substrates, while ethanol, acetate, glycerol and carbon dioxide form the products. This set of reactions is then used to obtain the elementary modes using the public domain Python-based software package ScrumPy [20]. Elementary modes can be evaluated for a given set of metabolic reactions that have equivalent overall stoichiometries in terms of the interconversion of external metabolites. The sets of elementary modes can be represented as (see [9, 24] for details)

$$\dot{M}\big|_{t_i} = A \cdot V(t_i), \tag{1}$$

where A and $\dot{M}$ represent the stoichiometry matrix of the elementary modes and the vector of accumulation rates of the external metabolites, respectively. V, the vector of fluxes of the elementary modes, is unknown and determined by EMA. The objective function can be either the maximization or minimization of the accumulation rate of a specific external metabolite (say, to maximize biomass). The linear optimization technique is used to solve Eq. 1, and it can be formulated to maximize the accumulation rate of the jth metabolite M_j, in other words [9]

$$\text{Max}\left(\frac{dM_j}{dt}\bigg|_{t_i}\right),$$

such that

$$\begin{aligned} \dot{M}' &= A' \cdot V' \\ 0 \le V_i' &\le \infty \quad \text{for all } i \end{aligned}, \tag{2}$$

where, A' is a matrix and M' is a vector obtained by eliminating the rows of the jth external metabolite from A and M, respectively. The accumulation rates of glucose, biomass, ethanol, glycerol, and acetate needed to determine the fluxes through EM in this study were obtained experimentally.

Materials and methods

Strains and growth conditions: the yeast strain used in this study was W303-1A (*MATa leu2-3/112 ura3-1 trp1-1 his3-11/15 ade2-1 can1-100 GAL SUC2*). Since this study was focused solely on the central carbon metabolism under osmotic shock, the yeast cells were grown in complete minimal (CM) medium [0.67% YNB (yeast nitrogen base without amino acids) and 2% glucose] and supplemented with uracil (50 mg/liter), tryptophan (50 mg/liter),

histidine (50 mg/liter), adenine (50 mg/liter), and leucine (250 mg/liter). A 6-liter bioreactor with a 1.1-liter working volume was inoculated with 100 ml of microbial broth. The temperature was maintained at 30°C, and the pH was held at 5.5 ± 0.3. Air was provided at a rate of 1.5 lpm. The culture was grown in normal medium until the exponential phase in the bioreactor, after which additional medium with the required NaCl concentration was added to make the final concentration 0.5 or 1 M NaCl.

Samples of 1 ml were taken periodically to determine the status of the fermentation. These were analyzed for extracellular concentrations of glucose, ethanol, and glycerol in HPLC. The dry cell weight was also measured. Since the low concentration of intracellular glycerol cannot be measured by HPLC, we used a chemical method to measure the glycerol, as described in [17]. For the intracellular glycerol measurements, the suspension was centrifuged at 5,000 rpm for 5 min and the supernatant was discarded. The method used to extract the intracellular glycerol in [16] was followed: the pellets were resuspended in 1 ml water and boiled for 10 min, and the supernatant was used for intracellular glycerol measurement.

Results

The central carbon metabolic network consists of 34 internal and 7 external metabolites and 41 stoichiometric reactions (see Table S2 of the ESM). The external metabolites considered were glucose, biomass, ethanol, glycerol, acetate, oxygen and CO_2. Using the ScrumPy software, 54 elementary modes of the network were obtained, which captured the stoichiometry relating the external metabolites in the network. As detailed in Table S3 of the ESM, 45 modes involved glucose and O_2 as substrates, while 9 modes used only glucose as the substrate. Biomass was associated with 48 modes, ethanol with 28, glycerol with 31, and acetate with 18.

Stoichiometric matrix A, constructed from the 54 elementary modes and the accumulation rates $\dot{M}$, are then used in the LP (Eq. 2) to obtain the fluxes of the EMs at different points in time and for different osmotic conditions during the fermentation. Although the network consists of seven external metabolites, the rank of the matrix A in Eq. 2 is 5, indicating that five independent measurements of accumulation rates would be sufficient to evaluate the molar balance.

In this work, we measured the accumulation rates of the following five metabolites: glucose, biomass, ethanol, acetate, and glycerol. Figure 1 shows the concentrations of these metabolites for growth in a medium containing 0, 0.5, and 1 M salt at various time points. It is clear that the rate of consumption of glucose decreases with increasing salt concentration (see Fig. 1a) due to a decreased growth rate, as observed in Fig. 1b. Further, the cells increased the production of glycerol necessary for their survival under high-osmolarity conditions (Fig. 1e), which results in decreased ethanol production (Fig. 1c). Thus, hyperosmotic stress adversely affects glucose consumption and ethanol and biomass production, while it stimulates glycerol production. At 5 h, the glucose uptake rate reduced from 14.77 mM/h for 0 M salt to 10.85 mM/h and 4.86 mM/h for 0.5 and 1 M salt, respectively. Glucose was completely consumed after 8, 10, and 14 h when the cells were exposed to media with 0, 0.5, and 1 M salt, respectively. The reduced uptake rates of glucose at increased salt concentrations correlate with the reduced growth rates of 0.18 h^{-1} and 0.10 h^{-1} for 0.5 M and 1 M salt relative to 0.23 h^{-1} under normal conditions. This was also reflected in the increased lag phases of 30 min and 3.5 h for 0.5 M and 1 M salt. The ethanol formation rate also diminished to 5.89 and 1.02 mM/h for 0.5 and 1 M salt, respectively, from 14.86 mM/h under normal conditions.

The above experimental data were used to estimate the accumulation rates at specific time points in order to determine the fluxes through various elementary modes. As indicated before, the rank of the stoichiometry matrix was 5, indicating that five accumulation rates were needed to evaluate the fluxes though the elementary modes. The five measured rates—those of glucose, biomass, ethanol, glycerol, and acetate—were used, along with biomass maximization in the LP formation (Eq. 2) as the objective function, to evaluate the fluxes through the EM. The flux distribution through the EM depends on the objective function, although it is constrained by the measured accumulation rates for the various extracellular metabolites. We used the objective function of biomass maximization to obtain the feasible flux distribution through each elementary mode at a given time point. The fluxes through the elementary modes obtained are represented in Figs. 2, 3, 4, and 5. The flux distribution in the original network can also be determined from the fluxes through the elementary modes [8]. Since the fluxes through elementary modes involving acetate were negligible, we report the fluxes through the remaining 35 elementary modes, which are associated with either glycerol, biomass, ethanol, or combinations of these. For clarity, we defined elementary modes 1–7 (which are associated with biomass) as group I, 8–12 (associated with biomass and ethanol) as group II, 13 (with ethanol) as group III, 14–15 (with glycerol) as group IV, 16–22 (with biomass and glycerol) as group V, 23–33 (with biomass, ethanol, and glycerol) as group VI, and 34–35 (with ethanol and glycerol) as group VII. All flux values are reported in units of mmol/gDCW/h.

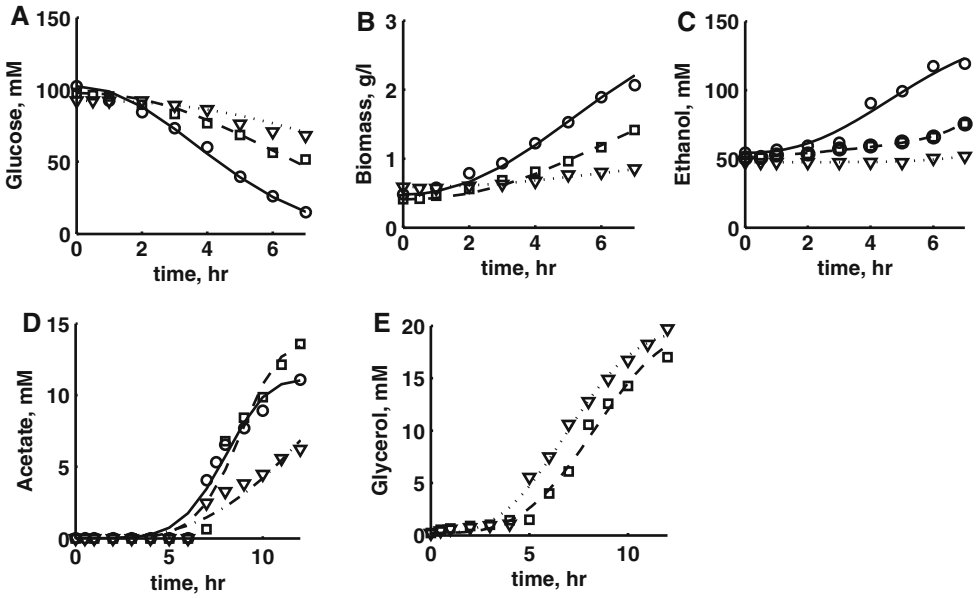

Fig. 1 The fermentation time course data for glucose (**a**), biomass (**b**), ethanol (**c**), acetate (**d**), and glycerol (**e**) for 0 M (*circles*, *solid line*), 0.5 M (*squares*, *dashed line*), and 1 M (*triangles*, *dotted line*) NaCl. *Symbols* represent experimental data, while *lines* represent fits to time courses

Figure 2a shows the average and the standard deviation of the glucose uptake rate through the different EMs at time points corresponding to 15 min, 30 min, 1 h, and 4 h for growth in a normal medium. As is evident from the figure, at 15 min, the modes corresponding to group I (producing only biomass) dominate over the other groups, while at 30 min, group II—encompassing modes with biomass plus ethanol—begin to dominate over the other groups. It is clear that the contribution from modes in group V, which includes glycerol along with biomass, is not active during growth under normal conditions. Moreover, about 96% of the glucose uptake rate is utilized for biomass formation at 15 min, which decreases to about 21% at 4 h. Figure 2b shows the distribution of glucose uptake rates through the EMs when the cells are exposed to 0.5 salt. Until 15 min, none of the EMs directed towards growth are active, indicating that the cells have ceased to divide and are in the adaptive phase. After 30 min, the EMs of groups I, II, and V become operational, with about 89% of the glucose uptake rate utilized for biomass formation, which is of the same magnitude as observed under normal conditions, indicating the end of the adaptation phase. After adaptation, all elementary modes are operational, indicating the simultaneous synthesis of biomass, glycerol, and ethanol. When cells are subjected to 1 M salt, none of the EMs are operational until about 1 h, with less than 0.023.6% of the net glucose uptake rate being utilized for biomass formation, indicating an extended adaptive phase under high osmotic shock (see also Fig. 2c). At 4 h, the biomass-related modes become operational, indicating that the cell begins to divide. The flux towards the biomass was 5% of the total uptake rate of glucose at 4 h. After adaptation, the percentage of glucose uptake towards biomass was less than 6% until the complete consumption of the glucose. Thus, as the salt concentration increases, the amount of glucose used for cell division drops as the glucose is utilized for the adaptation process.

The net uptake rate of the glucose, which represents the sum of the glucose uptake rates across the 35 EMs, continuously increases from 3.21 mmol/gDCW/h at 15 min to 8.39 mmol/gDCW/h at 4 h when cells are grown in the normal medium. It is clear from Fig. 2a that only modes pertaining to groups I, II, and III, which correspond to elementary modes directed towards biomass, biomass and ethanol, and ethanol alone, respectively, were operational. As expected, under normal conditions, EMs 14–35 corresponding to glycerol synthesis were not operational. At 0.5 M salt (Fig. 2b), the net uptake rate of the glucose decreases to 0.52 mmol/gDCW/h at 15 min and is about threefold lower than that under normal conditions at 4 h. For 1 M salt, it reduces further to 0.11 mmol/gDCW/h at 15 min and 1.55 mmol/gDCW/h at 4 h. Thus, as the salt concentration increases, the glucose uptake rate decreases, indicating a reduced metabolic rate. Moreover, when the cells are exposed to 0.5 M salt, the EM 15 corresponding to glycerol synthesis alone is active at 15 min, but at 30 min, all 35 modes—including those related to biomass and ethanol—become operational, indicating the end of the adaptive phase. In the case of growth in a medium containing 1 M NaCl, the adaptive phase is extended until 3 h (see Fig. 2c). The contribution of the glucose uptake to the biomass under normal conditions is shown in Fig. 3a in terms of the specific growth rate. It can be seen that the EMs associated with biomass and ethanol production are

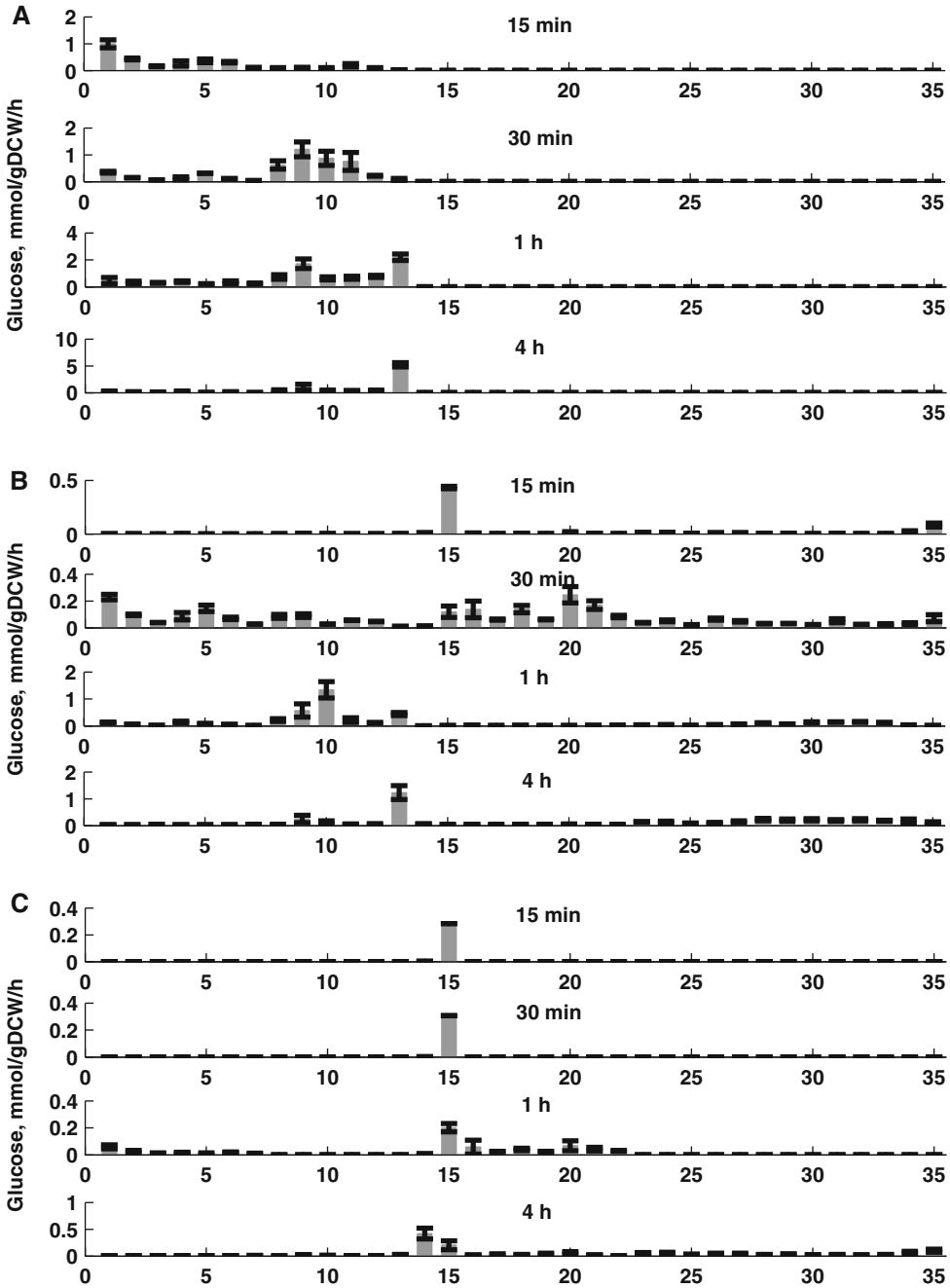

Fig. 2 Histogram of the distribution of glucose rates through various elementary modes for the metabolic network of *Saccharomyces cerevisiae*. Fluxes are in mmol/gDCW/h. Salt concentration: **a** 0 M, **b** 0.5 M, **c** 1 M. Elementary modes 1–7 are associated with biomass, 8–12 with biomass and ethanol, 13 with ethanol, 14–15 with glycerol, 16–22 with biomass and glycerol, 23–33 with biomass, ethanol, and glycerol, and 34–35 with ethanol and glycerol

operational for 0 M salt throughout the fermentation. Under an osmotic shock of 0.5 M NaCl, the flux through each EM becomes minimal at 15 min (see Fig. 3b), with only 5% of the glucose uptake rate directed towards the biomass. Subsequently, at 30 min, EMs belonging to groups I, II, III, and IV become operational, resulting in an increased fraction of the glucose uptake rate which is equivalent to that seen under normal conditions. Under the hyperosmotic stress of 1 M NaCl, at 15 min, only 1.4% of the glucose uptake rate is used for biomass formation, which increases to 5% at 4 h, indicating poor growth at high osmolarity (Fig. 3c).

Figure 4a shows the distribution of fluxes through EMs directed towards glycerol synthesis for cells growing under normal conditions. It is clear that trace amounts of glycerol are visible at 4 h. However, after being subjected to an osmotic shock corresponding to 0.5 M NaCl, the elementary mode 15, representing glycerol synthesis, dominates over all other modes at 15 min (see Fig. 4b), with 62% of the glucose uptake rate being utilized for net glycerol

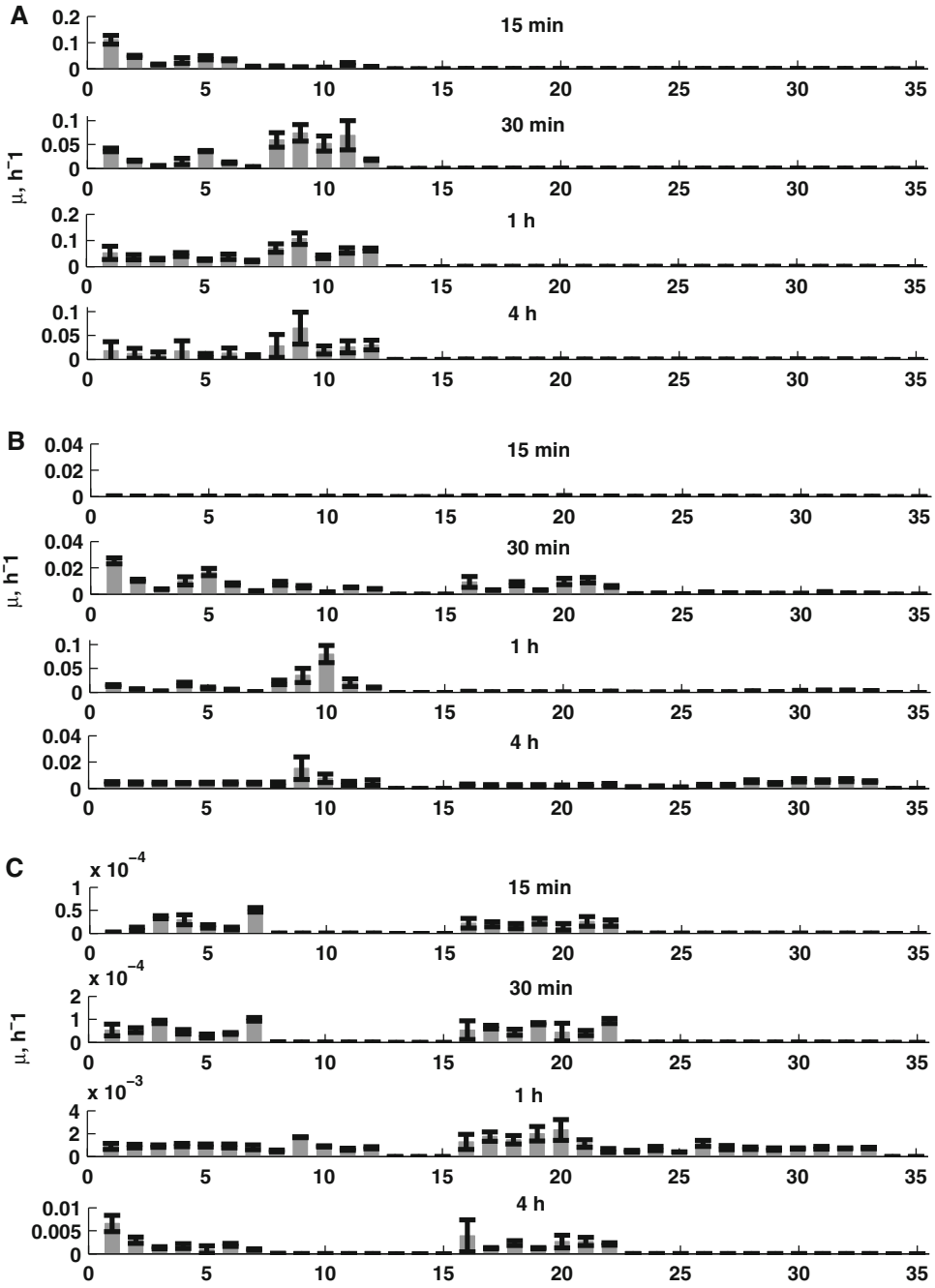

Fig. 3 Histogram of the distribution of biomass rates through various elementary modes for the metabolic network of *Saccharomyces cerevisiae*. Fluxes are in mmol/gDCW/h. Salt concentration: **a** 0 M, **b** 0.5 M, **c** 1 M. Elementary modes 1–7 are associated with biomass, 8–12 with biomass and ethanol, 13 with ethanol, 14–15 with glycerol, 16–22 with biomass and glycerol, 23–33 with biomass, ethanol, and glycerol, and 34–35 with ethanol and glycerol

synthesis. Subsequently, at 30 min, the elementary modes belonging to groups II, IV, and V, all of which involve glycerol synthesis, also become operational, resulting in an enhanced fraction of 28% of the glucose uptake rate being directed towards glycerol synthesis. Under hyperosmotic stress from 1 M NaCl, EM 15 dominates over the entire 4 h period, indicating that the adaptation phase extends over a longer duration (Fig. 4c).

Under normal conditions, the glucose uptake rate is directed towards ethanol purely through group II modes, which consist of biomass and ethanol (see Fig. 5a). Further, the net rate of ethanol synthesis increases with time: only 8% of the glucose is converted to ethanol at 15 min, and 37% of the glucose is converted to ethanol at the end of 4 h. The flux distribution for ethanol for different EMs when the cells are exposed to 0.5 and 1 M salt, are shown in Fig. 5b and c, respectively. It should be noted that, in addition to group II modes, modes consisting of glycerol synthesis along with ethanol in groups IV and V are also operational. However, the fraction of the net glucose uptake rate directed towards ethanol drops dramatically, since the carbon in glucose is utilized for the synthesis of glycerol and acetate.

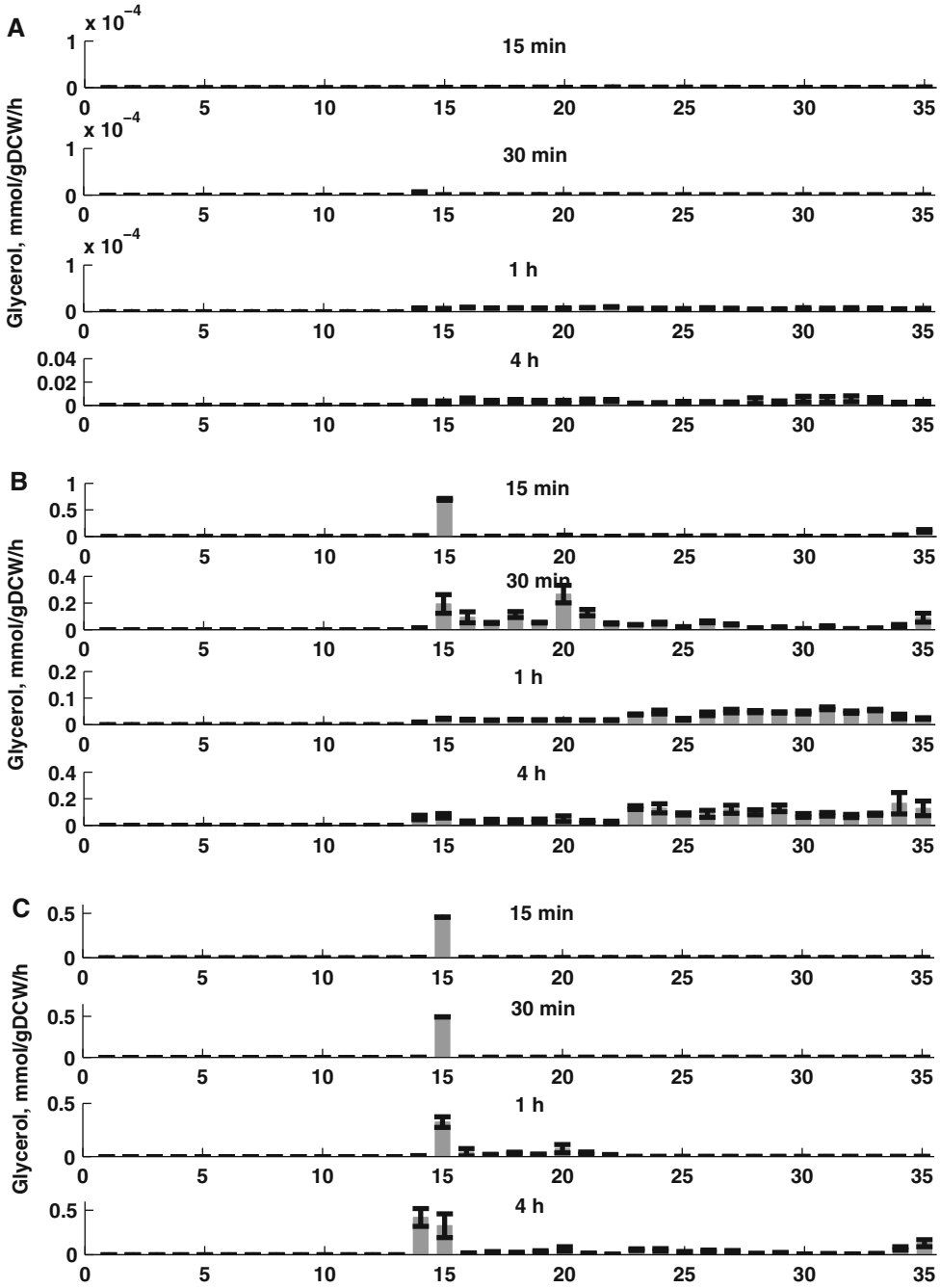

Fig. 4 Histogram of the distribution of glycerol rates through various elementary modes for the metabolic network of *Saccharomyces cerevisiae*. Fluxes are in mmol/gDCW/h. Salt concentration: **a** 0 M, **b** 0.5 M, **c** 1 M. Elementary modes 1–7 are associated with biomass, 8–12 with biomass and ethanol, 13 with ethanol, 14–15 with glycerol, 16–22 with biomass and glycerol, 23–33 with biomass, ethanol, and glycerol, and 34–35 with ethanol and glycerol

EMA is also useful in that it can quantify the rates of the reactions through the original network from which the EMs were derived. Figure 6 shows the metabolic flux distributions for *S. cerevisiae* at 15 min. It can be observed that for normal growth, the normalized flux through the pentose pathway is about eightfold higher than that for growth in a medium with 0.5 M salt concentration. The flux through the pentose pathway is negligible for the case with 1 M salt concentration. Significant flux towards the pentose pathway indicates high-growth conditions. Thus, when the cells are adapting to the osmotic shock, the flux through the pentose pathway is downregulated. Further, the flux towards the glycolytic pathway at GA3P is about twofold higher under normal conditions compared to that observed in the case with 0.5 M salt. This lowered flux through the glycolytic pathway observed under hyperosmotic shock is channeled towards glycerol synthesis through DHAP. Thus, a substantial flux value is observed for the reversible conversion of GA3P to DHAP (indicated by the negative flux value in Fig. 6), while under normal growth a flux value of 62 is noted for the conversion of DHAP to GA3P. This results in high normalized fluxes of 129 and 157

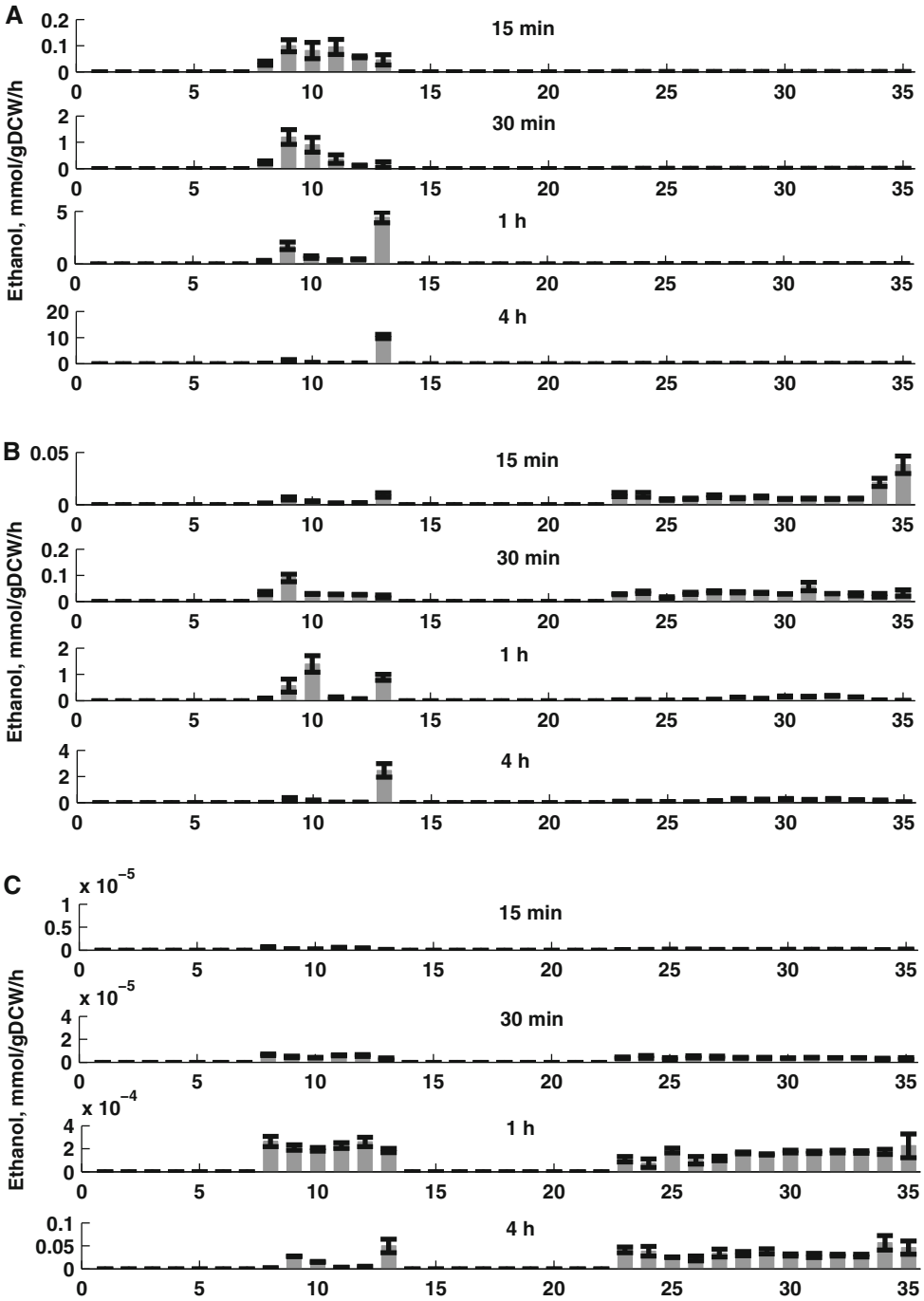

Fig. 5 Histogram of the distribution of ethanol rates through various elementary modes for the metabolic network of *Saccharomyces cerevisiae*. Fluxes are in mmol/gDCW/h. (Salt concentration: **a** 0 M, **b** 0.5 M, **c** 1 M. Elementary modes 1–7 are associated with biomass, 8–12 with biomass and ethanol, 13 with ethanol, 14–15 with glycerol, 16–22 with biomass and glycerol, 23–33 with biomass, ethanol, and glycerol, and 34–35 with ethanol and glycerol

towards glycerol during the first 15 min of the adaptation process. It should also be noted that the conversion of pyruvate to acetaldehyde and to oxaloacetate is lowered due to osmotic shock. However, the overall flux through the TCA cycle remains constant and invariant to osmotic stress. The net flux through ATP consumption is lowered with osmotic shock, implying a higher maintenance cost due to the stress.

Figure 7 shows the flux distribution in the metabolic network at $t = 30$ min for cells growing in media containing 0, 0.5, and 1 M salt. The flux through the pentose pathway for the case with 0.5 M salt increased and is only twofold lower than that for normal growth. This implies that the growth phase has resumed for cells growing in 0.5 M salt. However, for the case of 1 M salt, the flux through the pentose pathway is low, indicating that the cells are still adapting to the high stress. This can also be observed for the flux for the conversion of DHAP to GA3P: while the flux value is positive for both normal conditions and for the case with 0.5 M salt, it remains

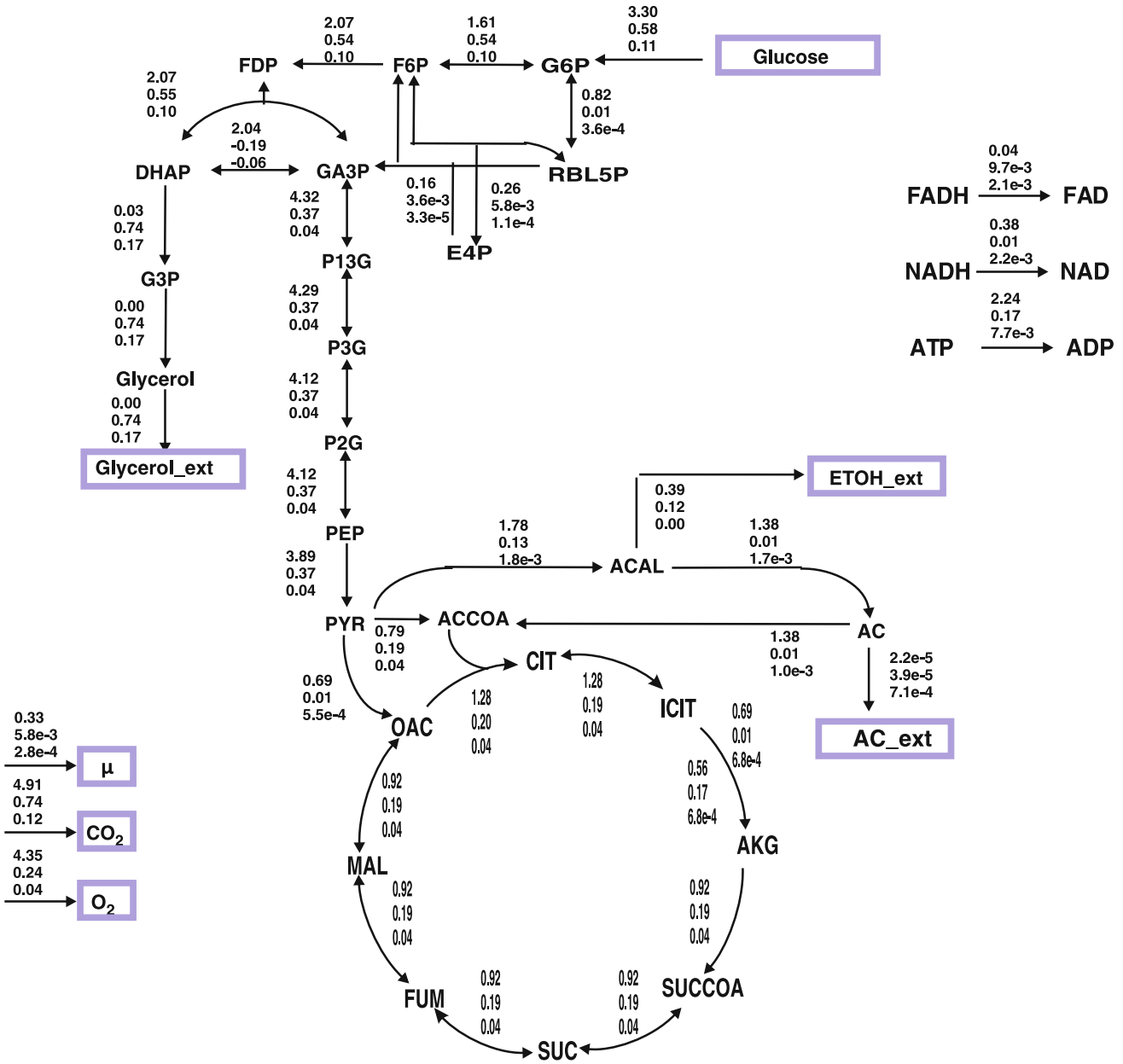

Fig. 6 Flux distribution map of *S. cerevisiae* at 15 min for osmotic shocks of 0, 0.5, and 1 M NaCl (*from top to bottom*). The fluxes are expressed in mmol/gDCW/h. For abbreviations, see Table S1 in the ESM

negative for the case with 1 M salt. At 30 min, it can be observed that the flux towards ethanol is also lowered for the cases with osmotic stress as compared to that observed for normal growth. 2.5- and 200-fold higher fluxes towards ethanol were observed for the case with normal growth as compared to that for growth in media containing 0.5 and 1 M salt, respectively, demonstrating the regulation of ethanol formation under stress. However, at $t = 4$ h, the cells growing under 1 M NaCl adapt to the osmotic shock, as seen from the flux distribution in Fig. 8. Here, the flux towards pyruvate is comparable to that observed under normal conditions. In this case, the ethanol accumulation, O_2 and ATP consumption, and TCA cycle fluxes are comparable for cells growing in media containing 0, 0.5, and 1 M NaCl. It should also be noted that at $t = 4$ h, the flux from DHAP to GA3P is positive even for the case with the highest osmotic stress.

NADH reoxidation is essential for energy production, which is required for cell division as well as for glycerol synthesis. To evaluate the effect of osmotic shock on NADH reoxidation, the flux through the NADH reoxidation reaction was compared at various salt concentrations

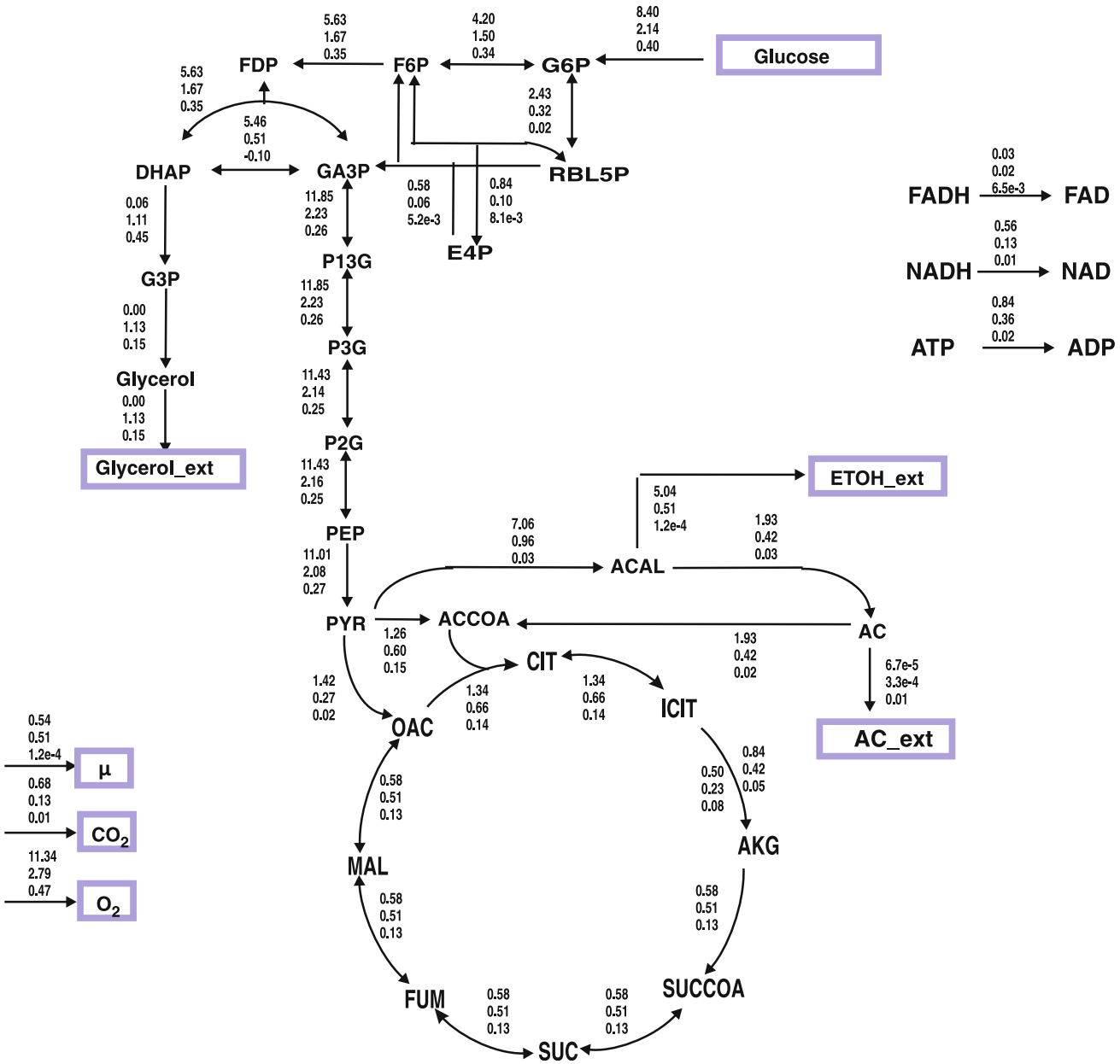

Fig. 7 Flux distribution map of *S. cerevisiae* at 30 min for osmotic shocks of 0, 0.5, and 1 M NaCl (*from top to bottom*). The fluxes are expressed in mmol/gDCW/h

and over time. It should be noted that NADH reoxidation occurs through three main reactions: the electron transport chain (ETC), glycerol synthesis, and ethanol synthesis. Table 1 lists the percentage contributions of the three mechanisms of NADH reoxidation under various osmotic conditions. As expected, at all time points, reoxidation mainly occurs through the ETC under normal conditions. The percentage reoxidation through ethanol formation increases to about 18% at 30 min and saturates beyond that time point. Glycerol synthesis does not contribute to NADH reoxidation. Under an osmotic shock of 0.5 M NaCl, about 50% of the reoxidation occurs through glycerol synthesis, with the remainder being shared between the ETC and ethanol synthesis at 15 min. At later time points, the contribution of the ETC increases with a concomitant decrease in percentage reoxidation due to both glycerol and ethanol synthesis. Under an osmotic shock of 1 M NaCl, about 70% of the reoxidation is through glycerol synthesis, which is 1.5 times that observed for 0.5 M NaCl. At later time points, the contribution of the ETC increases in a similar manner to that observed for the case with 0.5 M NaCl. The total NADH reoxidation rate increased over time for all three cases, indicating that there is a higher ATP requirement as cells adapt and enter the exponential growth phase. However, at

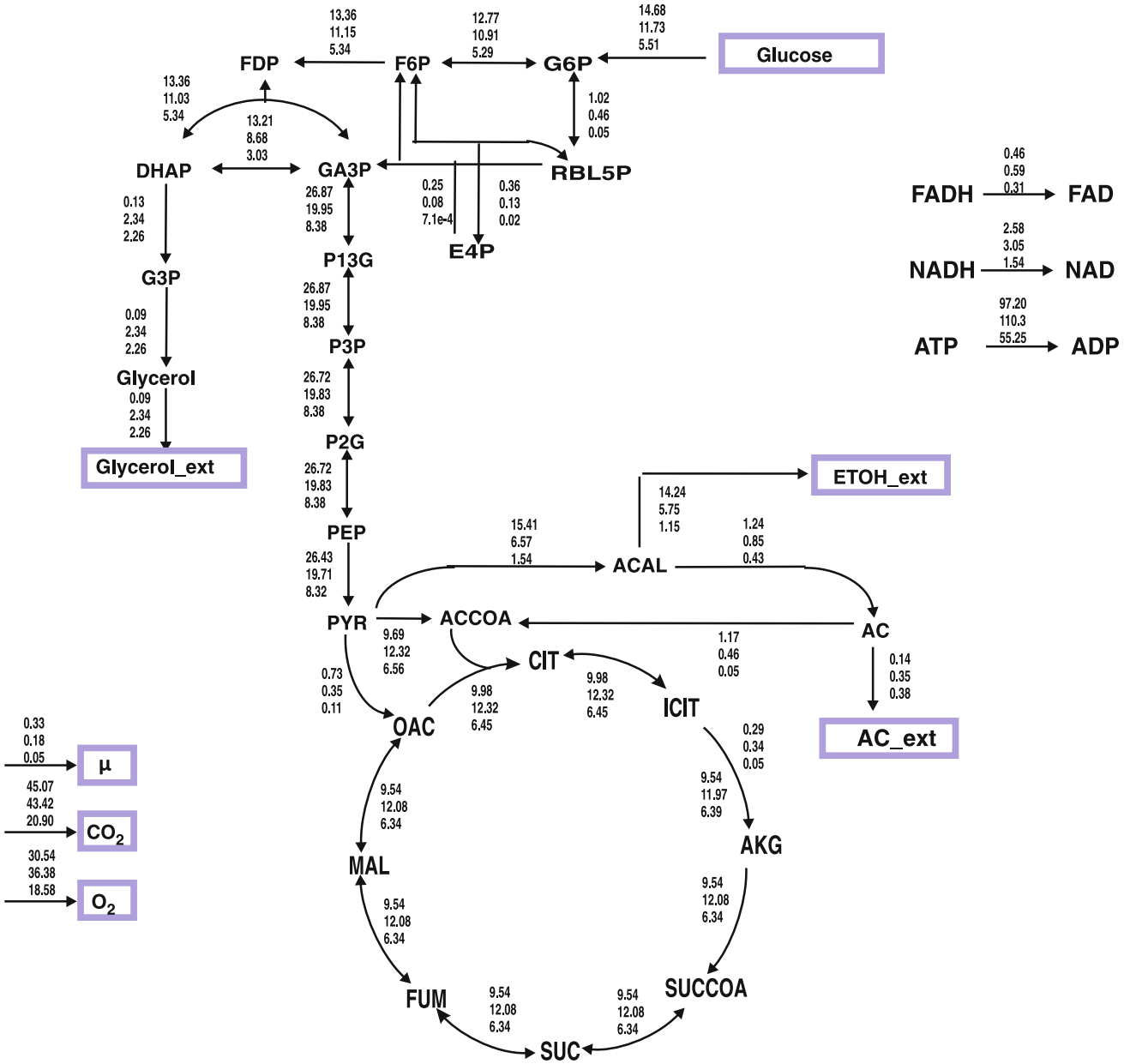

Fig. 8 Flux distribution map of *S. cerevisiae* at 4 h for osmotic shocks of 0, 0.5, and 1 M NaCl (*from top to bottom*). The fluxes are expressed in mmol/gDCW/h

Table 1 Percentage NADH reoxidation through the electron transport chain (ETC), glycerol synthesis, and ethanol synthesis under different osmotic conditions

% NADH reoxidation	15 min			30 min			4 h		
	0 M	0.5 M	1 M	0 M	0.5 M	1 M	0 M	0.5 M	1 M
ETC	96	30	32	82	77	86	81	90	92
Glycerol	0	46	68	0	16	14	0	3	6
Ethanol	4	24	0	18	7	0	19	7	3
Total (mM/h/DCW)	9.1	1.6	0.3	27.7	7.2	1.1	75.4	80.9	40.6

each time point, the total NADH reoxidation decreased as the salt concentration increased, indicating a lower ATP requirement due to poor growth under osmotic shock. Thus, under osmotic shock, during adaptation, the NADH reoxidation is mainly due to glycerol synthesis, while during growth post-adaptation, the reoxidation is primarily due to the ETC.

The flux distribution can be used to study the flux ratio at the key nodes, namely G6P (glucose 6-phosphate), DHAP (dihydroxyacetone phosphate), PYR (pyruvate), and ACAL (acetaldehyde), as shown in Table 2. At 15 min, the G6P node shows that 25% of the flux is directed towards the pentose pathway under normal conditions, while only 3% and 0.3% of the flux are observed to flow towards the pentose pathway at 0.5 and 1 M NaCl, respectively, indicating that growth is arrested upon osmotic shock. Thus, under stress, the glycolytic pathway is preferred, with almost 98% of the carbon flux passing through it. The flux through the DHAP node towards pyruvate synthesis is about 98% under normal conditions, indicating that glycerol synthesis is shut off almost entirely. Under 0.5 M NaCl, the flux ratio towards pyruvate is negative, indicating that GA3P is converted to DHAP. In this case, 134% of the net flux is channeled towards glycerol. A similar situation for the flux ratios is apparent for 1 M NaCl, with 160% of the influx directed towards glycerol synthesis. At the pyruvate node, under normal conditions, the flux ratio towards acetaldehyde is 50%, while the remainder is equally divided between acetyl co-enzyme A and oxalic acid. Under shock, most of the flux is directed towards acetyl co-enzyme A, with ratios of 54% and 93% for 0.5 and 1 M NaCl, respectively. For the acetaldehyde node, the flux towards acetate is high under both normal and hyperosmotic stress conditions.

At 30 min (see the flux values in Fig. 7), the flux towards the pentose phosphate pathway for cells growing under 0.5 M NaCl increases, indicating that growth has resumed, while that through the glycolytic pathway decreases relative to that at 15 min. On the other hand, at 1 M NaCl, the flux towards the pentose pathway at 30 min is only 7%, indicating that the cells are yet to completely adapt to the shock. For the DHAP node at 30 min, the flux towards the glycolytic pathway is 36% for cells under an osmotic shock of 0.5 M NaCl, which indicates that more ATP is needed for growth, which confirms that the cells have adapted to the osmotic shock. However, for 1 M, the flux towards the glycolytic pathway is negative, with a net flux ratio of 128% towards glycerol. It is clear from Table 2 that, at the pyruvate node, the flux ratio towards acetaldehyde is greatest for 0.5 M NaCl, similar to that observed for normal osmotic conditions. The flux ratio distribution for the four nodes at 4 h (see Fig. 8 for the flux values) is also shown in Table 2. It can also be observed that at the DHAP node, the flux towards the glycolytic pathway is now positive (57%), and only 43% is directed towards glycerol. This indicates that the cell has adapted to 1 M NaCl at 4 h.

Another advantage of EMA is that the elementary modes can be used to obtain a feasible phenotypic space for various objective functions such as biomass and glycerol by relaxing two of the five stoichiometric constraints needed to evaluate the molar balance. We chose the accumulation rate of glucose, which was fixed at 100 mmol/gDCW/h. The consumption rate of O_2 and the accumulation rate of CO_2 were varied over specific ranges to obtain a feasible phenotypic space. The LP in Eq. 2 was solved for various objective functions to obtain the phenotypic space. The feasible ranges for the accumulation rates of O_2 and CO_2 were found to be 50–470 mmol/gDCW/h and 80–480 mmol/gDCW/h, relative to the glucose uptake rate, respectively. These values therefore provide the bounds for the maximum and minimum rates of CO_2 accumulation and O_2 consumption to yield a feasible phenotype. The maximum biomass yield obtained from the analysis was 11.6, with normalized O_2 consumption and CO_2 accumulation rates of 106 and 112, respectively. Figure 9a shows

Table 2 Flux ratios at different nodes in the metabolic network under different osmotic conditions

Nodes	Flux towards	15 min			30 min			4 h		
		0 M	0.5 M	1 M	0 M	0.5 M	1 M	0 M	0.5 M	1 M
G6P	PP	25	3	0.33	29	15	7	7	4	1
	Glycolytic	50	94	99	50	70	85	87	93	96
DHAP	Pyruvate	98	−34	−58	97	36	−28	99	79	57
	Glycerol	1.5	134	160	1.2	67	128	1	21	43
PYR	ACCOA	20	54	93	12	29	58	37	62	79
	ACAL	46	37	4	64	46	13	58	33	19
	OAC	18	3	1.2	13	10	10	3	2	1
ACAL	Ethanol	22	91	0	72	53	0	92	88	75
	Acetate	78	13	99	27	45	1	8	13	25

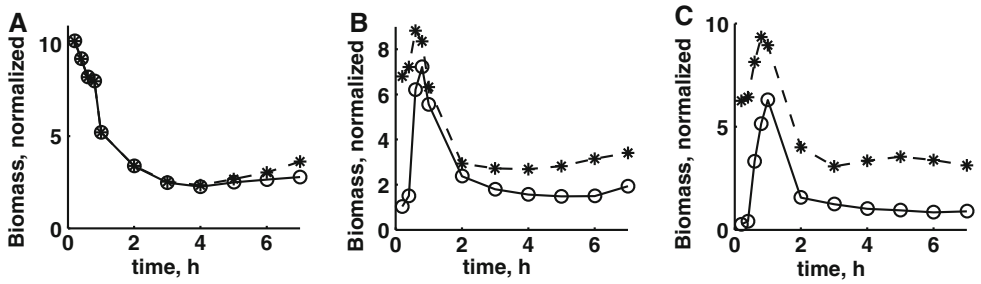

Fig. 9 Comparison of experimentally measured biomass formation rates with the maximum feasible rates obtained by solving the LP (Eq. 2) using three constraints: glucose, O_2, and CO_2 for 0 M (**a**), 0.5 M, (**b**) and 1 M (**c**) salt, respectively. *Open circles* indicate experimental data, *asterisks* indicate maximum feasible values

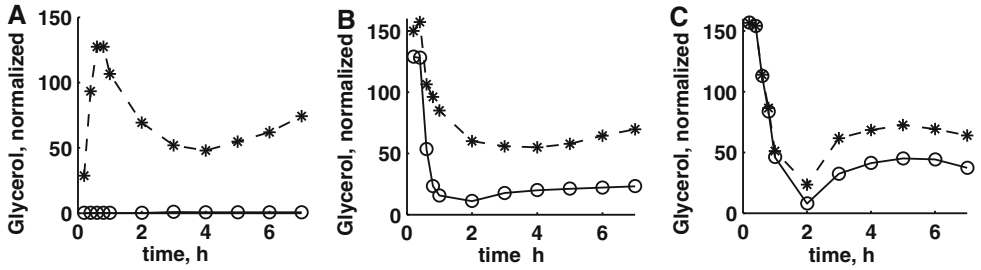

Fig. 10 Comparison of experimentally measured glycerol formation rates with the maximum feasible rates obtained by solving the LP (Eq. 2) using three constraints: glucose, O_2, and CO_2 for 0 M (**a**), 0.5 M, (**b**) and 1 M (**c**) salt, respectively. *Open circles* indicate experimental data, *asterisks* indicates maximum feasible values

the experimentally obtained time course of biomass for normal growth conditions, which were compared with that for the maximum feasible biomass formation rate. It is clear from Fig. 9a that during the first 5 h, the organism optimizes biomass, since the experimental data lies within the region of maximum feasible biomass formation rate. The experimental data beyond $t = 5$ h deviate from the optimum, and are lower than the maximum feasible biomass formation rate due to the formation of ethanol. However, when the cells were grown in a medium containing 0.5 M NaCl, the experimentally observed biomass formation rate was suboptimal during the first hour (see Fig. 9b). During the first half hour, corresponding to the adaptive phase, the observed biomass formation rate was sevenfold lower than the maximum feasible rate under an osmotic shock from 0.5 M NaCl. After adaptation, the experimental data was closer to the maximum rate, but it deviated further beyond 2 h, although it was only about twofold lower (Fig. 9b). It should be noted that the maximum feasible biomass accumulation rates for cells grown at 0 M, 0.5 M, and 1 M NaCl were 10, 7.5, and 6 (see Fig. 9a, b, and c), respectively, relative to a glucose uptake rate of 100 mmol/gDCW/h, indicating that the growth was constrained by the lower O_2 consumption rate under stress. To compare the experimentally observed glycerol synthesis rate with the maximum feasible rate, the above analysis was repeated by maximizing the glycerol formation rate. The feasible ranges of the O_2 consumption and CO_2 accumulation rates are 1–500 mmol/gDCW/h and 82–500 mmol/gDCW/h, respectively, when maximizing glycerol synthesis. The maximum glycerol accumulation rate was noted to be 160, which corresponds to the stoichiometry of elementary mode 15 (see Table S3 of the ESM). Figure 10a shows a comparison between the experimentally obtained glycerol formation rate and the maximum feasible glycerol formation rate for normal growth with 0 M salt in the medium. As expected, the experimental values show only minimal glycerol synthesis rates, while the maximum feasible for normal conditions was 135 relative to the glucose uptake rate at 1 h, indicating that under normal conditions the cells do not activate glycerol synthesis. Figure 10b shows a comparison between the experimentally measured glycerol accumulation rate and the maximum feasible rate when the cells are exposed to 0.5 M NaCl. The figure shows that the initial glycerol formation rates until $t = 30$ min are 0.8-fold of those obtained for the maximum feasible glycerol synthesis rate. The experimental data deviated beyond 30 min post-adaptation, and were threefold lower than the maximum glycerol synthesis rate. When the cells were grown on a medium containing 1 M NaCl, the experimental glycerol synthesis rate was equal to the maximum feasible rate until $t = 2$ h, indicating that the cells optimally produce glycerol during the initial adaptive phase (see Fig. 10c). However, the experimental data deviated beyond $t = 2$ h and were

about 1.6-fold lower than the maximum feasible rate. It was also noted that during the first half hour of the adaptive phase, the cells produce glycerol at the stoichiometrically maximum feasible rate of 150 mmol/gDCW/h. The maximum experimentally observed rates for glycerol were 0.05, 125, and 150 mmol/gDCW/h for 0, 0.5, and 1 M salt, respectively.

Discussion

Yeast remodels its metabolism under hyperosmotic conditions to channel the carbon towards glycerol production, which is essential for the adaptation process [2–4]. To obtain a deeper understanding of the metabolic readjustment that occurs under hyperosmotic conditions, we have quantified the network using elementary mode and flux balance analyses. Five experimentally determined accumulation rates—those of glucose, biomass, ethanol, glycerol, and acetate—were used to obtain the flux distribution of the elementary modes. Although five measurements were sufficient to evaluate the molar balance of external metabolites, the flux distributions for elementary modes were not unique for the different maximization criteria, reported as the mean value of each operational elementary mode using different maximization criteria.

Groupwise analysis of the elementary modes under normal and hyperosmotic conditions clearly showed that different groups were operational under normal and hyperosmotic conditions. This is due to the fact that the hyperosmotic stress reconfigures the metabolism with enhanced glycerol production. The increased glycerol level is responsible for the adaptation and survival of the cells under conditions of increased osmotic shock. The enhanced glycerol formation results in reduced yields of biomass and ethanol and thus decreased rates of elementary modes of the groups associated with them under such conditions. The rates of the elementary modes for glucose consumption also diminish with increased salt concentration. The inhibitory effect on glucose uptake rate may be a combined effect of volume shrinkage and reduced efficiency of biomass and ethanol production. It is interesting to note that under severe osmotic stress, cells metabolize glucose through only one elementary mode, which shows the maximum theoretical yield of glycerol during the initial extended lag phase during adaptation. All elementary modes that produce glycerol use oxygen and the TCA cycle to fulfill the energy requirements as well as to achieve redox balance. Further, in the post-adaptation phase, the elementary modes that become operational always involve glycerol along with other products in order to maintain the pool of glycerol needed for to survive persistent osmotic shock. In the normal medium, the elementary modes that operate involve either biomass or biomass with ethanol. Thus, cells use distinct groups of elementary modes under normal and hyperosmotic conditions.

The flux distributions in the elementary modes were then used to determine the reaction fluxes in the original metabolic network. The flux towards the pentose phosphate pathway reduced during the adaptation period, which indicated that the hyperosmotic stress temporally arrests the cell cycle. It is interesting to note that, although the overall glucose consumption decreases with increased osmolarity, as observed in our experiments and also reported in [18, 27], the net glycolytic flux increased relative to the glucose uptake rate. Further, under stress, the carbon flux from glucose toward G3P increased, and that toward pyruvate decreased, resulting in enhanced glycerol production. The low rates of NADH reoxidation in the adaptive phase indicate low metabolic activity under osmotic shock in this phase. In the post-adaptation phase, the increased reoxidation of NADH implies that cells use NADH simultaneously for glycerol and ATP formation. The diminished O_2 utilization and ATP formation under increased osmotic stress indicate that the cells minimize energy and CO_2 production, which helps when increasing glycerol formation. After adaptation, the flux values observed for the hyperosmotic conditions are comparable to those seen for the normal case, implying a return to the normal metabolic state. The nodal flux distribution indicates that the GA3P is converted to DHAP and results in a decreased flux towards the TCA cycle when the cells are exposed to increased osmotic stress. Further, at the PYR node, an increased flux toward ACCOA with increasing osmolarity was observed. The analysis was then used to determine the feasible solution space for fluxes of elementary modes using linear optimization strategy. Using this methodology, the ability of the network to achieve a specific objective function was characterized [9]. Three accumulation rates—those for glucose, oxygen, and carbon dioxide—were used to evaluate the ability of the network to produce maximum biomass or glycerol. Various other factors, such as the stoichiometry of the elementary modes, and the aerobic and anaerobic routes, also helped to constrain the solution space. A comparison of the experimental accumulation rates for biomass and glycerol synthesis with those observed under optimal conditions indicated that biomass formation was optimal during the exponential growth phase with an absence of glycerol formation for normal growth. However, in the late exponential phase, the carbon flow towards ethanol and acetate results in suboptimal biomass formation. Under osmotic stress, the cells do not grow optimally, with growth rates being less than those of wild-type cells.

Conclusion

Adaptation to osmotic shock in *S. cerevisiae* is a coordinated process at various levels regulating signaling, genetic, and metabolic pathways. Information is transmitted through the signaling pathway to the cell cycle, gene regulation, and to several nodal points in the metabolism. The coordinated processes greatly alter fluxes in the metabolic network of *S. cerevisiae* under hyperosmotic stress to regulate the synthesis of various metabolites. We quantified the metabolic network using the elementary mode approach to capture these alterations during osmotic stress. Results indicate that the cells metabolize glucose by different sets of elementary modes under normal and hyperosmotic conditions. The elementary modes associated with biomass formation are operational during exponential growth in the normal medium, while the elementary modes involving glycerol production are operational in the medium with high osmolarity. The analysis demonstrated that fluxes at several nodal points are regulated to achieve the optimal synthesis of glycerol. Elementary mode analysis is thus a potential tool to characterize the phenotypic responses under various environmental cues.

References

1. Albertyn J, Hohmann S, Prior BA (1994) Characterization of the osmotic-stress response in *Saccharomyces cerevisiae*: osmotic stress and glucose repression regulate glycerol-3-phosphate dehydrogenase independently. Curr Genet 25(1):12–18
2. Blomberg A (1995) Global changes in protein synthesis during adaptation of the yeast *Saccharomyces cerevisiae* to 0.7 M NaCl. J Bacteriol 177(12):3563–3572
3. Blomberg A, Adler L (1989) Roles of glycerol and glycerol-3-phosphate dehydrogenase (NAD+) in acquired osmotolerance of *Saccharomyces cerevisiae*. J Bacteriol 171(2):1087–1092
4. Brewster J, de Valoir T, Dwyer N, Winter E, Gustin M (1993) An osmosensing signal transduction pathway in yeast. Science 259(5102):1760–1763
5. Çakir T, Kirdar B, Ülgen KÖ (2004) Metabolic pathway analysis of yeast strengthens the bridge between transcriptomics and metabolic networks. Biotechnol Bioeng 86(3):251–260
6. Carlson R, Fell D, Srienc F (2002) Metabolic pathway analysis of a recombinant yeast for rational strain development. Biotechnol Bioeng 79(2):121–134
7. Carlson R, Srienc F (2004) Fundamental *Escherichia coli* biochemical pathways for biomass and energy production: identification of reactions. Biotechnol Bioeng 85(1):1–19
8. Gayen K, Gupta M, Venkatesh KV (2007) Elementary mode analysis to study the preculturing effect on the metabolic state of *Lactobacillus rhamnosus* during growth on mixed substrates. In Silico Biol 7(2):123–139
9. Gayen K, Venkatesh KV (2006) Analysis of optimal phenotypic space using elementary modes as applied to *Corynebacterium glutamicum*. BMC Bioinform 7:445
10. Gianchandani EP, Papin JA, Price ND, Joyce AR, Palsson BO (2006) Matrix formalism to describe functional states of transcriptional regulatory systems. PLoS Comput Biol 2(8):902–917
11. Gustin MC, Albertyn J, Alexander M, Davenport K (1998) Map kinase pathways in the yeast *Saccharomyces cerevisiae*. Microbiol Mol Biol Rev 62(4):1264–1300
12. Hohmann S (2002) Osmotic stress signaling and osmoadaptation in yeasts. Microbiol Mol Biol Rev 66(2):300–372
13. Klamt S (2006) Generalized concept of minimal cut sets in biochemical networks. Biosystems 83(2–3):233–247
14. Klamt S, Gilles ED (2004) Minimal cut sets in biochemical reaction networks. Bioinformatics 20(2):226–234
15. Klamt S, Saez-Rodriguez J, Lindquist JA, Simeoni L, Gilles ED (2006) A methodology for the structural and functional analysis of signaling and regulatory networks. BMC Bioinform 7:1–26
16. Klipp E, Nordlander B, Kruger R, Gennemark P, Hohmann S (2005) Integrative model of the response of yeast to osmotic shock. Nat Biotechnol 23(8):975–982
17. Lambert M, Neish AC (1950) Rapid method for estimation of glycerol in fermentation solution. Can J Res 28:83–89
18. Loray MA, De Figueroa LIC, Hofer M (1998) Effect of salt stress on sugar uptake in osmotolerant yeasts. Folia Microbiol (Praha) 43(2):204–206
19. Papin JA, Price ND, Wiback SJ, Fell DA, Palsson BO (2003) Metabolic pathways in the post-genome era. Trends Biochem Sci 28(5):250–258
20. Poolman MG (2006) ScrumPy: metabolic modelling with Python. Syst Biol 153(5):375–378
21. Poolman MG, Fell DA, Raines CA (2003) Elementary modes analysis of photosynthate metabolism in the chloroplast stroma. Eur J Biochem 270(3):430–439
22. Reed RH, Chudek JA, Foster R, Gadd GM (1987) Osmotic significance of glycerol accumulation in exponentially growing yeasts. Appl Environ Microbiol 53(9):2119–2123
23. Schilling CH, Letscher D, Palsson BO (2000) Theory for the systemic definition of metabolic pathways and their use in interpreting metabolic function from a pathway-oriented perspective. J Theor Biol 203(3):229–248
24. Schuster S, Dandekar T, Fell DA (1999) Detection of elementary flux modes in biochemical networks: a promising tool for pathway analysis and metabolic engineering. Trends Biotechnol 17(2):53–60
25. Schuster S, Fell DA, Dandekar T (2000) A general definition of metabolic pathways useful for systematic organization and analysis of complex metabolic networks. Nat Biotechnol 18(3):326–332
26. Schuster S, Hilgetag C (1994) On elementary flux modes in biochemical reaction systems at steady state. J Biol Syst 2:165–182
27. Singh KK, Norton RS (1991) Metabolic changes induced during adaptation of *Saccharomyces cerevisiae* to a water stress. Arch Microbiol 156(1):38–42
28. Trinh CT, Carlson R, Wlaschin A, Srienc F (2006) Design, construction and performance of the most efficient biomass producing *E. coli* bacterium. Metab Eng 8(6):628–638
29. van Gulik WM, Heijnen JJ (1995) A metabolic network stoichiometry analysis of microbial growth and product formation. Biotechnol Bioeng 48(6):681–698
30. Vanrolleghem PA, de Jong-Gubbels P, van Gulik WM, Pronk JT, van Dijken JP, Heijnen S (1996) Validation of a metabolic network for *Saccharomyces cerevisiae* using mixed substrate studies. Biotechnol Prog 12(4):434–448
31. Wlaschin AP, Trinh CT, Carlson R, Srienc F (2006) The fractional contributions of elementary modes to the metabolism of *Escherichia coli* and their estimation from reaction entropies. Metabol Eng 8(4):338–352